Application of a Full Potential Method for Predicting Supersonic Flowfields and Aerodynamic Characteristics

Kenneth M. Jones*
NASA Langley Research Center, Hampton, Virginia

A nonlinear aerodynamic prediction technique that solves the conservative full potential equation has been applied to the analysis of three waverider configurations. This technique was selected based on its capability to analyze the off-design characteristics of the waveriders. Very good correlations were achieved with surface pressure data for both the Mach 4 elliptic-cone waverider and the Mach 6 caret-wing derivative. Off-design Mach number and angle-of-attack pressure correlations were very good for the elliptic-cone waverider. The range of correlation with data exceeded that expected based on the theory limitations. A surface pressure integration routine was demonstrated, and agreement between predicted aerodynamic forces and experimental force data for the Mach 4 waverider was excellent. Analysis of a nonconical waverider configuration was initiated where a discrete input option is used to achieve the computational gridding. Preliminary analysis of this configuration indicates that the correct shock location will be predicted.

Introduction

THE most commonly used aerodynamic prediction techniques for the analysis of supersonic flow over three-dimensional surfaces can be classified in two basic categories. Methods based on supersonic linear theory are applicable to slender configurations at low to moderate supersonic Mach numbers ($M=1.2$ to $M=2.5$). These methods are restricted by assumptions of isentropic flow, small disturbances, and potential flow and have limited use for analysis at high angle of attack and/or high supersonic Mach numbers. The second category includes the high supersonic and hypersonic Mach number ($M>4$) panel methods that use tangent cone, tangent wedge, or similar analysis methods. However, the panel methods are themselves limited in their usefulness because they do not account for interference between surfaces. Despite their inherent restrictions, both categories have successfully analyzed complex three-dimensional geometries with minimum computer time and cost. More sophisticated methods of nonlinear analysis based on the solution of the Euler or Navier-Stokes equations exist, but their use as practical prediction techniques for aircraft design is not yet a reality. Also, these techniques often require an increased level of effort by the user to perform an analysis of even elementary configurations. Thus, a need exists for a nonlinear supersonic technique that will produce accurate results for complex geometries while making efficient use of computational resources and minimizing the required level of user sophistication.

One particular class of nonlinear supersonic analysis methods is becoming an attractive candidate to bridge the gap between simple linearized methods and the complex Euler solvers. These are the full potential solvers which have matured into successful supersonic prediction techniques and are now becoming competitive with the above-mentioned methods. It is appropriate to note that the user of a full potential method should be aware of the isentropic limitations of the theory that may restrict its use. In general though, the theory is expected to perform well as long as the local product of Mach number M and flow deflection angle δ is less than one ($M\delta \leq 1$). Another criterion used as a rule of thumb is that the Mach number normal to the shock should be less than about 1.4. To date, full potential methods have shown accurate agreement with experimental data at low to moderate supersonic Mach numbers ($M=1.7$ to $M=3$).[1,2] The full potential method of Ref. 2 has also been used to demonstrate the capability to predict flow characteristics for high supersonic/hypersonic Mach number flows. Success has been achieved in predicting surface pressure distributions on various configurations ranging from simple bodies of revolution to a conical supersonic wing-body configuration.[2,3] Work continues in several areas to develop the full potential solvers into more efficient analysis tools for complex aircraft geometries.[4-6]

This paper will show the application of the full potential method described in Refs. 2 and 4 to analyze several waverider configurations for which experimental data are available for comparison. The paper will illustrate the accuracy of the method for this class of configurations and demonstrate its use in the Mach 3 to 6 speed regime. Initially, however, some discussion of the method itself and its flexibility is appropriate.

Full Potential Analysis Method

Briefly, the technique of Ref. 4 is based on the full potential equations written in conservative form in order to conserve mass across shock waves as well as throughout the flow. The technique also employs characteristic signal propagation theory to correctly control density biasing for treatment of shocks (including embedded shocks) and mixed elliptic-hyperbolic cross flow. One of the primary advantages of the method is the generation of the computational grid prior to the actual solution of the equations. This allows verification of the numerical grid (distribution, clustering, etc.) before proceeding with the solution. This has proved invaluable in detecting potential grid problems. The solution procedure for the equations does not place any specific requirements on the geometry or physical grid system.

This method is still in the developmental and validation stage. Over the past year considerable progress has been achieved in the complexity of the geometries analyzed, the accuracy of the results obtained, the reduction of execution time, and the ease of the geometry input process. Initially, the code was used to successfully analyze simple cones and bodies of revolution at angle of attack.[3] Recent improvements now allow grid generation for complex geometries such as realistic

Presented as Paper 83-1802 at the AIAA Applied Aerodynamics Conference, Danvers, Mass., July 13-15, 1983; submitted Sept. 24, 1984; revision received Jan. 29, 1985.

*Aerospace Engineer, High-Speed Aerodynamics Division. Member AIAA.

nonconical wing bodies, which can be analyzed with relative ease.[2,4] For conical geometries the grid arrangement is identical in each marching plane and the conical flowfield is assumed to have converged, once the change in root mean square density in the marching plane is reduced below a user-specified criterion (typically 10^{-5}). For nonconical geometries the computational grid must be generated at each marching plane since the configuration no longer has identical cross-sectional shapes. An initial data plane is established near the nose of the configuration by assuming a conical nose shape. Nonconical marching follows, and at each nonconical marching plane the density is iterated to convergence before proceeding to the next plane.

The underlying philosophy behind the development of the method aims at making it into one that can be implemented easily and that produces the type of results often desired by those working on such current research problems as surface pressure distributions and aerodynamic coefficients. Steps have been taken throughout the code development process to ensure the generality of the input necessary to execute the method. This has led to the separation of the equation solution procedure and the grid generation process. The user can execute the code without a detailed knowledge of the actual solution procedure; all that is required for input is the geometric definition of the configuration. This definition can be in the form of an analytic expression or can be obtained through the use of any one of a number of geometry generation techniques, such as a computer-aided design (CAD) package.

Several improvements have been added to the grid generation portion of the code to make this a more versatile analytic technique. The need for these modifications arose as a result of the application of the full potential method to waverider configurations. References 4 and 5 contain the details of two major improvements that control the grid density over the configuration. The "double-grid" system allows the user to break the cross-sectional grid into two regions, which proves extremely helpful when analyzing sharp leading edges and allows different grid clustering in the two regions. The second improvement, which was used for one of the waverider configurations, is a method to create the body-fitted grid given the geometry cross-section point data along the configuration. The user supplies the cross-sectional geometry in the form of discrete points, which are then input to an elliptic grid solver. This method results in a minimum of input required on the part of the user and is general enough to be used for a variety of configurations (especially where an analytic definition cannot describe the shape). The use of these two techniques will be illustrated during the analysis portion of the paper.

For some configurations it is desirable to vary the grid densities at different locations along the configuration. Reference 4 describes the respace option, which automatically interpolates the solution at a given cross section from an $m \times n$ grid to a $p \times q$ grid (e.g., 20×20 to 30×40). This has proved extremely useful for cases in which a coarse grid is sufficient for a portion of the configuration but a fine grid is eventually required to maintain the solution accuracy. A typical example might be a wing-body configuration in which a coarse grid is used for the forebody region, but a fine grid is required for the wing-body portion of the configuration.

Results to date using this full potential method have compared surface pressure distributions with experimental data and available Euler solutions; however, pressure data are not always available, and researchers are interested in the performance characteristics of the configurations. Therefore, the full potential code has been modified to allow integration of the inviscid surface pressures. This produces an estimate of the inviscid forces for the configuration and, when combined with skin-friction estimates, it is possible to check the correlation between the nonlinear analysis and experimental force data. The waverider configurations examined include two conical derivatives and a nonconical design.

Waverider Configurations

Performance requirements for high-speed missiles have led to renewed interest in waverider configurations, particularly waveriders derived from conical shapes.[7,8] Waveriders meet the missile requirements for a slender, flat, volumetric efficient configuration that offers relatively high lift-to-drag ratios (L/D) to achieve the desired range at the required speeds. Typically, these vehicles are designed to have a lift-producing lower surface and a low drag, often freestream, aligned upper surface. Reference 8 emphasizes the fact that a void exists in techniques capable of analyzing these shapes, particularly at angle of attack and off-design Mach numbers. The full potential analysis method of Ref. 4 will be used to analyze three waverider configurations, both to validate the method and to suggest its use in an area where other methods are currently lacking. The first configuration to be examined is a Mach 4 design from Ref. 7.

Waverider Results

Elliptic-Cone Waverider—Surface Pressure Calculations

A Mach 4 waverider derived from the flow past an elliptic cone at zero angle of attack, referred to as the elliptic-cone waverider, and shown in Fig. 1, was selected to determine the accuracy of the full potential method. The bottom centerline of this model is at an angle of 16.8 deg relative to the freestream velocity vector. The upper surface is a flat plate with 20-deg anhedral. The computational grid created by the grid generation routine is shown in Fig. 2. This waverider, as well as the other waveriders, was analyzed more efficiently and accurately using the double-grid modification due to the sharp leading edge and the appearance of two regions of flow on the vehicle (i.e., lift-producing lower surface, freestream upper surface). For this configuration, the two grid regions are bounded by the upper surface and the lower surface, with the dividing line being the ray extension of the upper surface. Grid generation is accomplished by prescribing points along the two surfaces and dividing line.

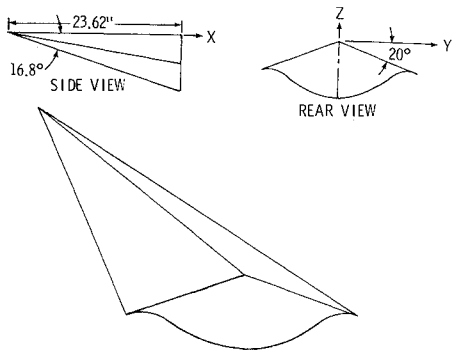

Fig. 1 Mach 4 elliptic-cone-derived waverider.

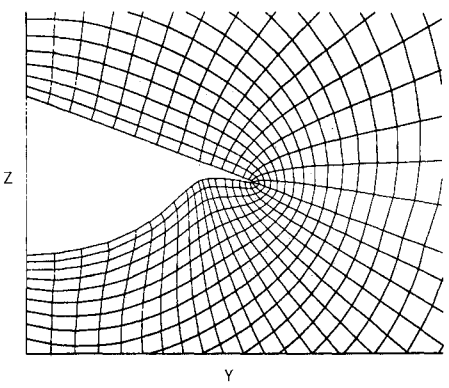

Fig. 2 Computational grid for a Mach 4 elliptic-cone waverider.

Comparison between experimental and calculated surface pressure coefficients is shown in Fig. 3 at the design point, Mach 4 and zero angle of attack. The agreement is quite good where experimental data are available; however, no data were taken in the tip region of the configuration. In addition to the surface calculations shown, flowfield calculations are also obtained. A typical plot of the flowfield pressure contours is presented in Fig. 4.

Off-design characteristics are of great interest to the researcher and, as stated in Refs. 7 and 8, most available analysis methods cannot accurately resolve the flowfields. The full potential method was used to investigate both on- and off-design Mach numbers at various angles of attack. Figures 5 and 6 compare calculated surface pressure results with experimental data for the waverider at a Mach number of 4 for various angles of attack ranging from -15 to 10 deg. Figure 5 shows the pressure distributions on the lower surface, and Fig. 6 the distributions on the upper surface. Recalling the inviscid, irrotational, isentropic limitations of potential theory, it is expected that as viscous effects become appreciable (e.g., separated flow) or when the assumption of isentropic flow is no longer valid, then deviation should be observed in the correlation with data. This is evident in Fig. 5. The comparison between theory and experiment is very good for low centerline flow deflection angles and becomes less accurate as the flow deflection angle is increased. As the flow deflection angle increases, the flow no longer approximates an isentropic flow, and the calculated surface pressures are much higher than the experimental results, because the code does not account for pressure losses through the shock due to entropy in the flow. However, at an angle of 5 deg and a flow deflection angle of 22 deg, the product $M\delta$ is about 1.5, which is much greater than one. As stated earlier, the method was expected to provide accurate results up to $M\delta \leq 1$ but, as shown by this example, the method is accurate even at larger values of the product $M\delta$. One way to improve the accuracy of the results at higher values of $M\delta$ is to use the technique of Ref. 9, which can be used to approximately correct the flowfield for entropy effects. This would require, however, that the current method be modified from a shock-capturing method to a shock-fitting method. These modifications were not employed for this study. Another important point is demonstrated in Fig. 6. The comparison of surface pressure on the upper surface is very good throughout the angle-of-attack range, even at those points where the lower surface pressure comparison are not very good. This is a result of the supersonic leading-edge condition.

Figures 7 and 8 again compare theory and experimental data over a range of angle of attack for Mach 3 and 5, respectively. For clarity, only comparisons of lower surface pressure coefficients are shown. The upper surface pressure coefficient comparisons are very similar to those shown in Fig. 6. Again,

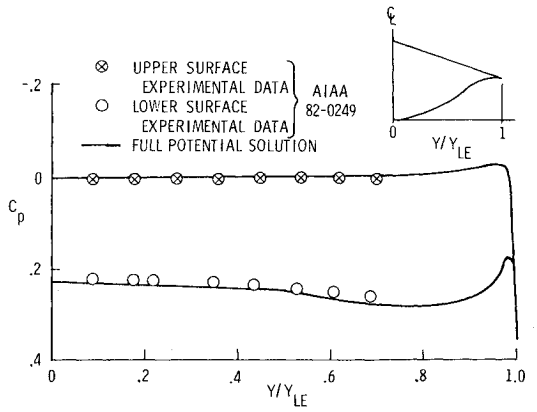

Fig. 3 Elliptic-cone waverider spanwise surface pressure distributions at $M=4.0$, $\alpha=0.00$.

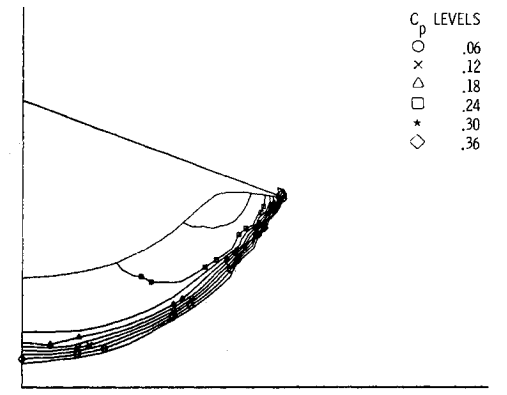

Fig. 4 Pressure contours for an elliptic-cone waverider at $M=4.0$, $\alpha=0.00$.

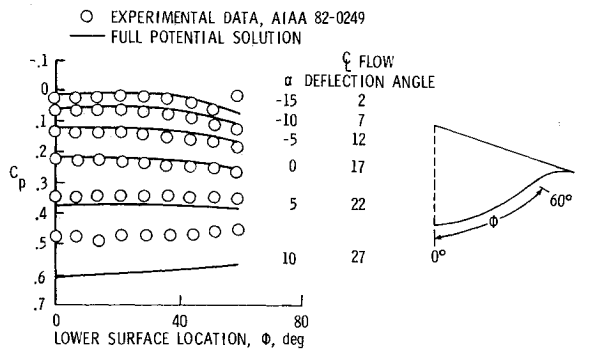

Fig. 5 Elliptic-cone waverider lower surface pressure distribution at $M=4.0$ and various angles of attack.

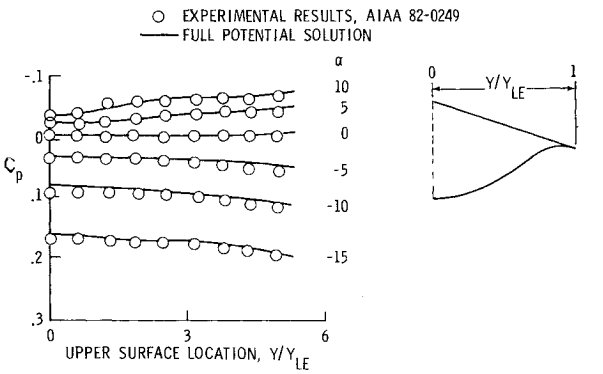

Fig. 6 Elliptic-cone waverider upper surface pressure distribution at $M=4.0$ and various angles of attack.

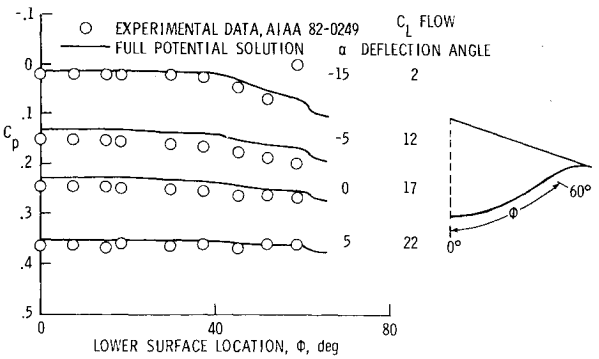

Fig. 7 Elliptic-cone waverider lower surface pressure distribution at $M=3.0$ and various angles of attack.

when the Mach number-flow deflection product becomes very high, the accuracy of the results declines. However, the correlation with the data remains quite accurate over a wide angle-of-attack range. Mach 3.5 and 4.5 cases were also calculated with correlation of results similar to those shown here.

Elliptic-Cone Waverider—Aerodynamic Forces

Pressure measurements are not always practical to obtain during experimental investigations; therefore, the estimate of a configuration's performance is based on experimentally obtained force data. Hypersonic analysis methods employing panel calculations often provide good correlation with experimental force data, even though the calculated pressure distributions are not accurate. The panel methods also neglect the mutual interference between computational elements and therefore may not be useful for configurations designed to benefit from this interference (e.g., waveriders). It would be desirable, then, to have an analysis tool that accurately predicts surface pressure distributions and shock locations and provides estimates of the forces acting on the configuration. As stated in the introduction, a surface pressure integration routine was added to the full potential method to provide estimates of the aerodynamic forces. To provide comparison with experimental force data, skin-friction estimates were obtained using the empirical methods in the Hypersonic Arbitrary Body Program (HABP).[10,11] The HABP skin-friction estimate for the elliptic-cone waverider used the tangent-wedge method for the tip or winglike region and tangent-cone method over the body. The local flow deflection angle and freestream Mach number determine the local pressures, using the Prandtl-Meyer equation to compute expansion pressures and either the oblique-shock conditions (tangent-wedge) or the conical-shock, isentropic compression conditions (tangent cone) to compute compression pressures. The skin-friction coefficient C_f was calculated from pressures using the skin-friction option of the HABP, which is based on the Spalding-Chi method.[12] The HABP C_f calculations were added to the inviscid full potential calculations for comparison with the elliptic-cone experimental data of Ref. 13.

Correlations with experimental data on the elliptic cone are shown in Figs. 9 and 10. For comparison purposes, HABP force estimates are also shown in the figures. As expected, the HABP C_L estimates are lower than the experimental data because HABP does not take into account the effect of interference pressures in the tip region. The agreement between full potential theory and experiment is very good up to a nearly 10-deg angle of attack. A similar trend is evident for drag coefficient C_D vs α. However, this is expected based on the distributions presented in Fig. 5. The calculated full potential pressures on the lower surface were consistently higher than the experimentally obtained pressures at 10-deg angle of attack. Therefore, the estimated forces should be higher than experiment. Figure 10 is a plot of lift-to-drag ratio L/D vs α. The comparison between full potential theory and experiment is quite good over the same angle of attack range as C_L and C_D.

Mach 6 Waverider

The previous analysis of the elliptic-cone waverider was incomplete as a result of the lack of experimental data in the tip region of the configuration. It is in this region that rapid flow changes are expected and are therefore of great interest to the designer and researcher. A thorough validation of the full potential analysis method requires an estimate of its ability to predict the flowfield in these regions. For this reason the Mach 6 waverider configuration reported in Ref. 8 and shown in Fig. 11 was also investigated. Experimental surface pressure data

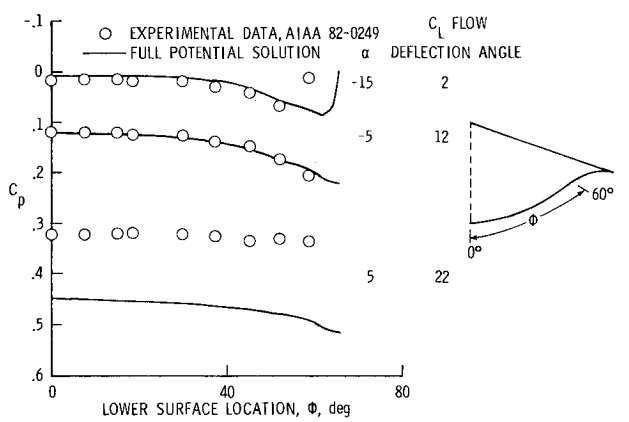

Fig. 8 Elliptic-cone waverider lower surface pressure distribution at $M=5.0$ and various angles of attack.

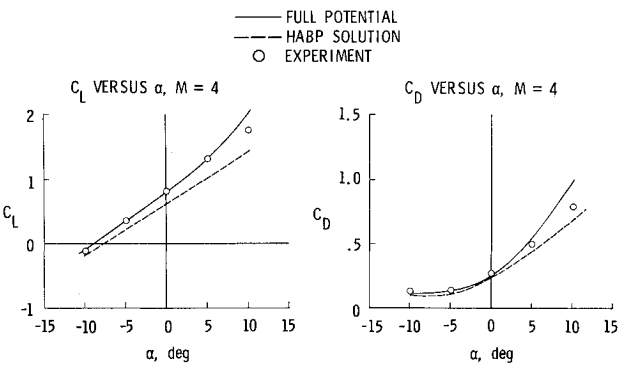

Fig. 9 C_L and C_D vs α for an elliptic-cone waverider at $M=4.0$.

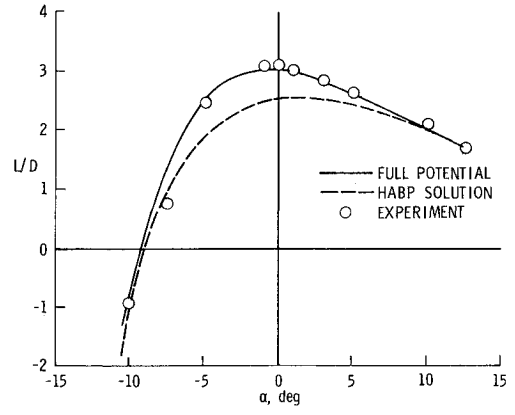

Fig. 10 L/D vs α for an elliptic-cone waverider at $M=4.0$.

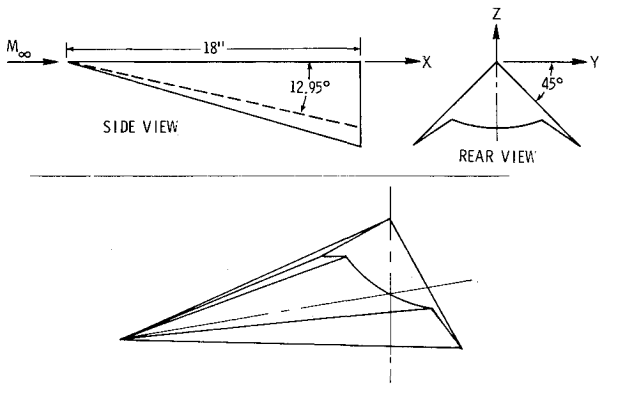

Fig. 11 Mach 6 cone-derived waverider configuration.

are available for this configuration in the wing-tip area and should allow a better estimate of the capabilities of the full potential method.

Results obtained on this configuration at its design point of Mach 6, zero angle of attack, are shown in Figs. 12 and 13. Figure 12 shows good agreement between the calculations and the experimental data along the lower surface up to about 70% of this semispan. After that point the correlation breaks down. The pressure contour plot, Fig. 13, helps to explain this behavior. The point at which the theoretical and experimental results diverge corresponds to the location at which the shock predicted by the full potential technique intersects the tip. Conical theory indicates that the predicted shock location below the body is accurate. It is possible that there will be a shock/boundary-layer interaction in the tip region, which can cause separation. Due to its limitations, the full potential method cannot predict separation or its effects. No details concerning the viscous nature of the flow were reported in Ref. 8; therefore, it is not possible to determine if boundary-layer separation did or did not occur in the tip region. For the Mach 4 elliptic-cone waverider, the bow shock was, for the most part, located outside the tip region or was just intersecting the tip. Reference 14 discusses both waverider configurations with respect to fully optimized waveriders and concludes that the Mach 6 waverider's performance (L/D) is less than that expected for an optimized waverider with the same volume, the base area A_b and the projected planform area S. The elliptic cone waverider, on the other hand, agrees well or is only slightly below the values predicted for a fully optimized waverider. Therefore, from a design standpoint it is desirable to avoid shock interactions inside the lip region, which will prevent the attainment of the best lift-to-drag ratio. A comparison between theoretical and experimental surface pressures along the lower surface for an angle-of-attack range is shown in Fig. 14. Again, there is good agreement with data up to a point in the tip region for Mach number angle-of-attack combinations where $M\delta$ is not much greater than one (e.g., for $M=6$, $\alpha=4$ deg, $M\delta$ is approximately 1.8).

Nonconical Waverider—Confined Flowfield Model

Validation of the full potential code to this point, as an analysis tool has centered on its use with conical geometries, in this case waverider configurations. An experimental investigation has been initiated at NASA Langley that will provide experimental data on a nonconical waverider concept called the confined flowfield (CFF) model. A sketch of this configuration is presented in Fig. 15. As shown in the side view, the curved upper surface does not lie along rays emanating from the nose, and therefore the geometry is not conical. Nonconical geometries either analytically defined or analytically fit have been previously studied.[2,4] An option is now available that allows analysis of nonconical geometries via the input of discrete numerical points. In general, obtaining an analytical fit for a configuration will be difficult and time-consuming; therefore, this option has proved extremely useful when analyzing complex configurations. Reference 5 shows the gridding achieved at various axial locations for a typical advanced fighter configuration (including grid generation around the wing-vertical tail juncture). The required cross-sectional input points may be obtained from a CAD system for input to the full potential grid solver. Due to the significance of the discrete numerical input option, a short discussion of how it was used to define the CFF model gridding is included.

The discrete numerical input option requires cross-sectional point information at user-prescribed stations along the con-

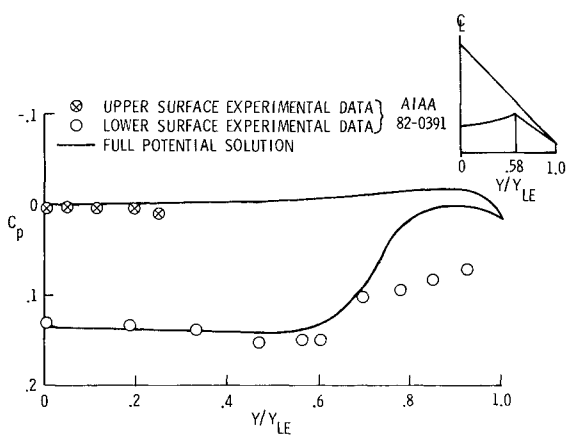

Fig. 12 Mach 6 cone-derived waverider spanwise surface pressure distribution at $M=4.0$, $\alpha=0.00$.

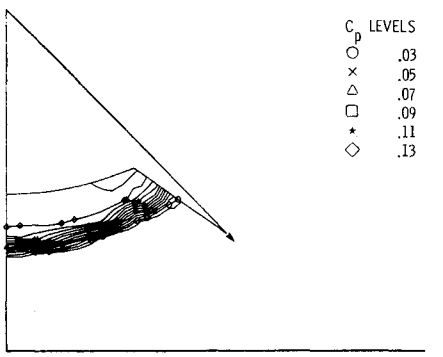

Fig. 13 Pressure contours for a Mach 6 waverider at $M=6.0$, $\alpha=0.00$.

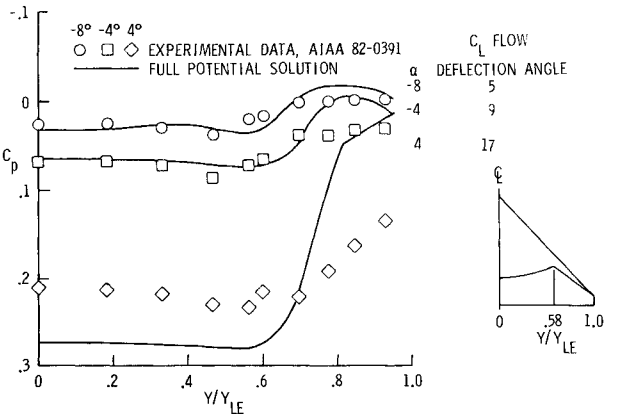

Fig. 14 Mach 6 waverider lower surface pressure distribution at $M=4.0$ and various angles of attack.

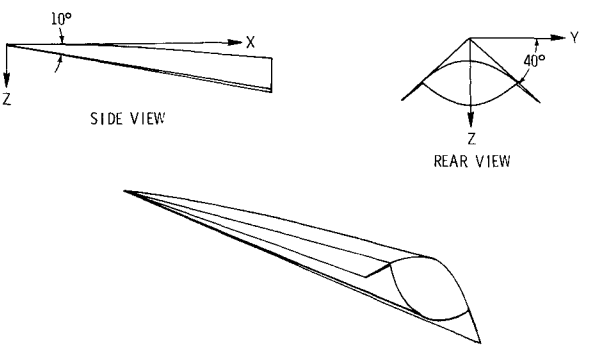

Fig. 15 Confined flowfield configuration.

figuration. The points are grouped into patches that are used to control the shape of the cross section and in turn the longitudinal lines of the configuration. For example, Fig. 16 shows a typical cross section for the CFF model. Three patches are used to define the section. One patch covers the upper surface, including the upper surface of the tip region. The second patch defines the lower surface of the tip, while the third patch fits the lower surface of the body. The number of cross sections required is arbitrary, and normally the same number of patches must be used for each cross section (this assumes similar cross-sectional shapes—for dissimilar shapes the configuration should be broken into sections, with each section modeled; then the respace option should be used to reset the grid at section boundaries). It is understood that an adequate definition of the configuration geometry will be required to analyze the flowfield successfully. Therefore, case should be exercised in the selection of section stations, and the patch end points should occur at each slope discontinuity in the cross section. With the cross section and patch information complete, the full potential grid solver automatically calculates the grid at each marching step via a simple cubic spline-ft routine.

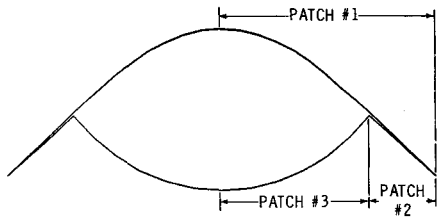

Fig. 16 Patch description on a typical confined flowfield cross section.

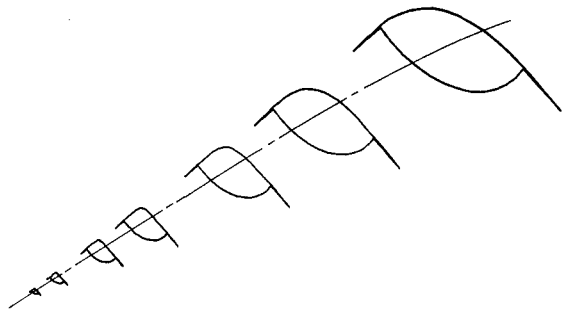

Fig. 17 GEMPAK generated cross sections of the confined flowfield model.

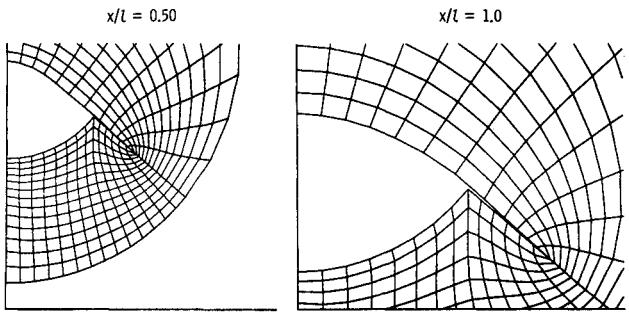

Fig. 18 Confined flowfield computational grid at $x/\ell = 0.5$.

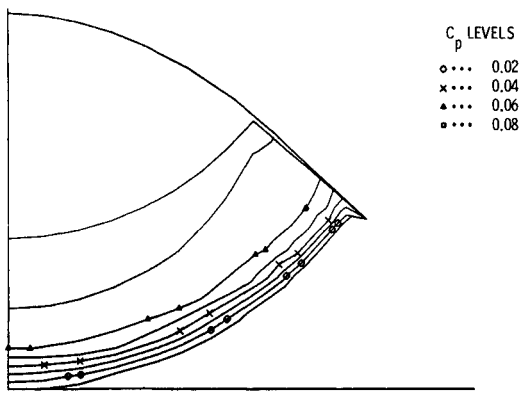

Fig. 19 Pressure contours for the confined flowfield model at $M = 6.0$, $\alpha = 0.00$.

The geometric definition of the CFF model was accomplished with a Langley-developed modeling package called GEMPAK.[15] The prescribed cross-section stations for the CFF model are shown in Fig. 17. The cross-section points for each station are output to a file and grouped into patches for input to the full potential grid routine. A typical computational grid is shown in Fig. 18.

Initially, based on the successful analysis of the two previous waveriders, no problems were anticipated with the CFF model. However, the CFF model has a very thin flat-platelike wing or tip region (see Fig. 18), which required additional modifications to the flow calculations in the tip region. The location at the tip, where the transformation metrics (physical to computational grid calculations) are computed, was modified. When the metrics are computed exactly at the sharp leading edge, the values can become singular and cause instabilities in the solution. To overcome this problem, the metrics are now evaluated a quarter of a mesh width outboard on the grid line extending from the tip. With this modification, the full potential method can proceed with the analysis of the CFF model.

Figure 19 shows the pressure contours at a station near the rear of the configuration for $M = 6$ and $\alpha = 0.42$ deg. Again, the waverider exhibits the characteristic shock pattern, which should produce the desired performance characteristics. Comparisons between shock angle calculations from the conical shock tables[16] for a 10-deg cone at $M = 6$ and $\alpha = 0$ deg and Fig. 19 verify that the shock is in the correct location with respect to the body.

The experimental investigation of the CFF configuration is ongoing, and force and moment data will be obtained over an angle-of-attack range. No pressure data will be gathered, but the full-potential force estimates will be compared with the experimental force data.

Conclusions

A nonlinear supersonic analysis code that solves the conservative full-potential equation was used to examine the inviscid flows over three waverider configurations. The full potential analysis code was shown to be extremely successful in computing both the on-design and off-design characteristics of the waveriders within the isentropic limitations of potential theory.

Very good correlation with experimental surface pressure data was achieved over a wide Mach number and angle-of-attack range. For the Mach 4 elliptic-cone waverider, the results did not break down until the centerline flow deflection angles exceeded 22 deg ($M\delta = 1.5$), well beyond what was expected based on theory limitations. The pressure correlations for the Mach 6 waverider were good up to the point on the surface where theory indicates a shock intersection in the lip region. The shock location was shown to be correct, and the breakdown in agreement with data was due to an apparent shock/boundary-layer interaction.

Integrated inviscid pressures predicted by the theory were summed with empirical skin-friction estimates to provide aerodynamic force estimates for the Mach 4 elliptic-cone waverider. Correlation with experimental force data was very good. The full potential analysis method now becomes a

strong candidate tool for the aerodynamic analysis of waverider configurations.

References

[1]Siclari, M. J., "Computation of Nonlinear Supersonic Potential Flow over Three-Dimensional Surfaces," *Journal of Aircraft*, Vol. 20, May 1983, pp. 462-468.

[2]Shankar, V. and Osher, S., "An Efficient Full Potential Implicit Method Based on Characteristics for Analysis of Supersonic Flows," *AIAA Journal*, Vol. 21, Sept. 1983, pp. 1262-1270.

[3]Shankar, V., "Conservative Full Potential Implicit Marching Scheme for Supersonic Flows," *AIAA Journal*, Vol. 20, Nov. 1982, pp. 1508-1514.

[4]Clever, W. C. and Shankar, V., "Nonlinear Potential Analysis Techniques for Supersonic/Hypersonic Configuration Design," NASA CR-166078, April 1983.

[5]Shankar, V., Rudy, S., and Szema, K., "Application of a Two-Dimensional Grid Solver for Three-Dimensional Problems," presented at the Mini-Symposium on Advances in Grid Generation-ASME Fluids Engineering Conference, June 20-22, 1982, published in bound volume #Z00222.

[6]Siclari, M. J., "Approximate Factorization Schemes for 3D Nonlinear Supersonic Potential Flow," AIAA Paper 83-0376, Jan. 1983.

[7]Jischke, M. C., Rasmussen, M. L., and Daniel, D. C., "Experimental Surface Pressures on Cone-Derived Waveriders for $M_\infty = 3$ to 5," *Journal of Spacecraft and Rockets*, Vol. 20, Nov.-Dec. 1983, pp. 539-545.

[8]Schindel, L. H., "Design of High Performance Hypersonic Missiles," AIAA Paper 82-0391, Jan. 1982.

[9]Siclari, M. J. and Visich, M., "Shock Fitting in Conical Supersonic Full Potential Flows with Entropy Effects," AIAA Paper 84-0261, Jan. 1984.

[10]Gentry, A. E. and Smythe, D. E., "Hypersonic Arbitrary-Body Aerodynamic Computer Program (Mark III Version)," Vol. I—User's Manual, Report DAC 61552 (available from DTIC as 851811), McDonnell Douglas Corp., April 1968.

[11]Gentry, A. E. and Smythe, D. N., "Hypersonic Arbitrary-Body Aerodynamic Computer Program (Mark III Version)," Vol. II—Program Formulation and Listings, Report DAC 61552 (available from DTIC as 851812), McDonnell Douglas Corp., April 1968.

[12]Spalding, D. B. and Chi, S. W., "The Drag of a Compressible Turbulent Boundary Layer on a Smooth Flat Plate With and Without Heat Transfer," *Journal of Fluid Mechanics*, Vol. 18, Jan. 1964, pp. 117-143.

[13]Rasmussen, M. L., Jischke, M. C., and Daniel, D. C., "Experimental Forces and Moments on Cone-Derived Waveriders for $M_\infty = 3$ to 5," *Journal of Spacecraft and Rockets*, Vol. 19, Nov.-Dec. 1982, pp. 592-598.

[14]Kim, B. S., Rasmussen, M. L., and Jischke, M. C., "Optimization of Waverider Configurations Generated from Axisymmetric Conical Flows," *Journal of Spacecraft and Rockets*, Vol. 20, Sept.-Oct. 1983, pp. 461-469.

[15]Stack, S. H., Edwards, C. L. W., and Small, W. J., "GEMPAK: An Arbitrary Aircraft Geometry Generator," NASA TP-1022, Dec. 1977.

[16]Sims, J. L., "Tables for Supersonic Flow Around Right Circular Cones at Zero Angle of Attack," NASA SP-3004, 1964.